Near-Infrared Imaging

DOI: 10.1002/ange.201206059

In Vivo Fluorescence Imaging with Ag_2S Quantum Dots in the Second Near-Infrared Region**

Guosong Hong, Joshua T. Robinson, Yejun Zhang, Shuo Diao, Alexander L. Antaris, Qiangbin Wang, and Hongjie Dai**

Cancer is one of the leading causes of human death in post-industrial countries. The mortality of cancer could be greatly reduced with the help of early detection and diagnosis and efficient monitoring of therapy.[1] Tomographic imaging techniques, such as computed tomography (CT), magnetic resonance imaging (MRI), and positron emission tomography (PET), benefit from unlimited penetration depth but have limited spatial resolution and are unable to visualize real-time dynamics owing to their long acquisition time.[2] Compared to tomographic imaging techniques, fluorescence-based optical imaging benefits from fast feedback as well as diffraction-limited spatial resolution, but is usually limited by tissue penetration of approximately 1 mm for fluorophores emitting in the visible (400–750 nm) or traditional NIR-I region (750–900 nm), because of tissue scattering of photons.[3] For example, fluorescein isothiocyanate (FITC, emission at approximately 520 nm) was used to label ovarian cancer, with a detection limit down to approximately 1 mm^3, only when the tumor body was resected and imaged ex vivo, because of the poor penetration and high scattering of visible-region fluorescence.[4] A new imaging method incorporating high spatial resolution, fast feedback, and deep tissue penetration is desired to advance medical science and practice through better tumor imaging.

Recently, fluorescence-based optical imaging in the second near-infrared window (NIR-II, wavelength 1.0–1.4 μm) has been shown to be useful for both in vitro[5] and in vivo[6] imaging with carbon nanotube fluorophores. Fluorescence imaging in NIR-II is more desirable over visible (450–750 nm) and traditional NIR-I imaging (750–900 nm) owing to reduced photon scattering, deeper tissue penetration, and lower autofluorescence.[7] However, one of the issues of NIR-II imaging remains the limited choices of NIR-II fluorophores, such as single-walled carbon nanotubes (SWNTs),[8] certain types of quantum dots (QDs),[9] and a handful of polymethine dyes.[10] Other problems with NIR-II fluorophores include the relatively low fluorescence quantum yields and poor biocompatibility, which limit their use for in vivo imaging with enough temporal resolution.[6a] Thus far, SWNTs are the only NIR-II fluorophores that have been used for in vivo imaging applications. Therefore, there is an urgent need for other brightly fluorescent and biocompatible NIR-II fluorescent probes for biological imaging both in vitro and in vivo. Herein, we report the use of a new NIR-II fluorophore, silver sulfide (Ag_2S) QDs[9a] for imaging xenograft tumors with high fluorescence quantum yield (15.5 %) of NIR-II emission at approximately 1200 nm. They are free of heavy metals (Cd, Hg, or Pb) and can be used to detect tumors with a high signal-to-background ratio through passive tumor targeting.

The Ag_2S QDs were synthesized in an organic phase according to a previously published method.[9a,b] The hydrophobic Ag_2S QDs were then coated with a surfactant dihydrolipoic acid (DHLA) and reacted with amine-functionalized six-armed PEG, using ethyl(dimethylaminopropyl) carbodiimide/*N*-hydroxysuccinimide (EDC/NHS) to afford highly water, buffer, and serum soluble 6PEG-Ag_2S QDs with an average diameter of approximately 5.4 nm (Figure 1 a,f and Supporting Information, Figure S2a–c). The 6PEG-Ag_2S QDs were soluble and physically stable for over ten months in phosphate buffered saline (PBS; Figure 1 b) while retaining high fluorescence in the 1.0–1.4 μm NIR-II region upon excitation at 808 nm (Figure 1 c). A UV/Vis/NIR absorption spectrum of the 6PEG-Ag_2S QD solution showed increasing absorption in the shorter wavelengths (Figure 1 d), which was consistent with previous publications.[9a] The photoluminescence versus excitation (PLE) spectrum of the 6PEG-Ag_2S QD solution revealed that the emission of Ag_2S QDs was centered at 1200 nm (Figure 1 e) and independent of excitation. The fluorescence quantum yield of 6PEG-Ag_2S QDs was determined as approximately 15.5 %.[11] The photostability of 6PEG-Ag_2S QDs was tested by continuous illumination of the 6PEG-Ag_2S QD solution with an 808 nm laser diode at 0.14 $W\,cm^{-2}$ (Figure S2d). The NIR-II photoluminescence (PL) intensity did decrease in the first 200 s, but then stabilized and remained over 50 % of its initial PL intensity over 0.5 h of continuous irradiation. Because the QDs were typically illuminated for less than 2 min during in vivo

[*] G. Hong,[+] Dr. J. T. Robinson,[+] S. Diao, A. L. Antaris, Prof. H. Dai
Department of Chemistry, Stanford University
Stanford, CA 94305 (USA)
E-mail: hdai@stanford.edu
Y. Zhang,[+] Prof. Q. Wang
Division of Nanobiomedicine and *i*-Lab, Suzhou Institute of Nano-Tech and Nano-Bionics, Chinese Academy of Sciences
Suzhou 215123 (P. R. China)
E-mail: qbwang2008@sinano.ac.cn
[+] These authors contributed equally to this work.

[**] This work is supported by NIH-NCI 5R01CA135109-02 to H. Dai, the Chinese Academy of Science "Bairen Ji Hua" program, the Chinese Academy of Science "Strategic Priority Research Program" (XDA01030200), the Chinese Ministry of Science and Technology (2011CB965004) and the National Science Foundation of China (20173225) to Q. Wang, and a Stanford Graduate Fellowship to G. Hong.

Supporting information for this article (experimental details) is available on the WWW under http://dx.doi.org/10.1002/anie.201206059.

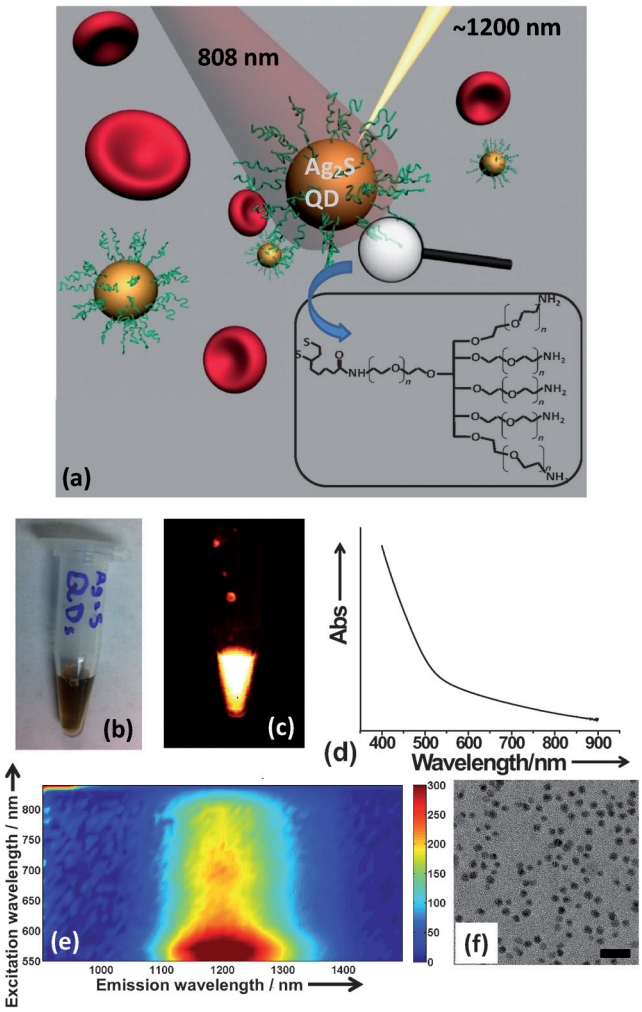

Figure 1. NIR-II Ag_2S quantum dots with branched PEG coating. a) A scheme showing the 6PEG-Ag_2S QDs that emit at 1200 nm upon excitation at 808 nm. Inset: chemical formula of the biocompatible PEG coating on the QDs. b) A white-light optical image of the 6PEG-Ag_2S QDs suspended in PBS at a concentration of 1.34 mg mL^{-1}. c) A photoluminescence (PL) image of the solution shown in (b). The excitation source was an 808 nm laser diode at 0.14 W cm^{-2} power density and the emission was collected from 1100–1700 nm. d) A UV/Vis/NIR absorption spectrum of the 6PEG-Ag_2S QD solution. e) A PL versus excitation (PLE) spectrum of the 6PEG-Ag_2S QD solution. Note the strong emission at 1200 nm that can be broadly excited from 550–820 nm. The scale bar on the right indicates the fluorescence intensity. f) A TEM image of 6PEG-Ag_2S QDs with an average diameter of 5.4 nm. Scale bar = 20 nm.

imaging, the 6PEG-Ag_2S QDs remained highly fluorescent in NIR-II without significant photobleaching during the imaging time.

With the stable and brightly fluorescent 6PEG-Ag_2S QDs, we injected a 200 μL solution of 6PEG-Ag_2S QDs at a concentration of 1.34 mg mL^{-1} (approximately 0.75 nmol per mouse) into the tail vein of a female BALB/c mouse with a subcutaneous xenograft 4T1 murine tumor located on the right hindlimb. Note, the injected dose of 0.75 nmol was on the lower side of the reported doses of other short-wavelength QDs intravenously administered for in vivo imaging (0.2–6 nmol per mouse).[12] Immediately after injection, fluorescence images over the NIR-II region (1.1–1.7 μm) were collected continuously by a two-dimensional InGaAs array detector (Princeton Instruments) to track the blood circulation of Ag_2S QDs in real time, with excitation by a laser at 808 nm at a power density of 0.14 W cm^{-2} (Figure S1), lower than the safe-exposure limit of 0.33 W cm^{-2} at 808 nm for small animals.[13] Supporting Movie 1 shows the video-rate NIR-II fluorescence images up to approximately 210 s post injection (p.i.) at a frame rate of 8.4 frames s^{-1}. 6PEG-Ag_2S QDs entered the venous blood from the tail vein and first circulated through the heart and lungs to be oxygenated in the first three seconds p.i. (Figure 2 a–c). This corresponded to the pulmonary circulation of the cardiovascular system, followed by systemic circulation in other organs such as the kidneys

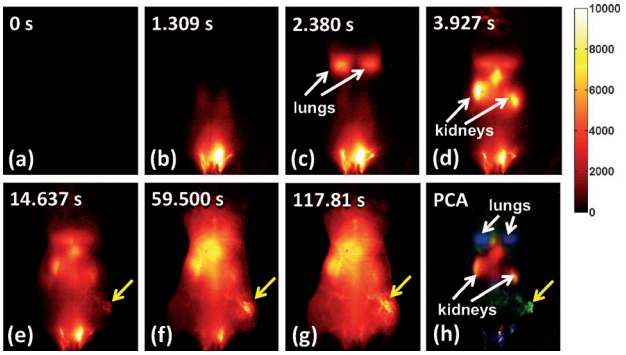

Figure 2. Time course of NIR-II fluorescence and dynamic contrast-enhanced image based on principal component analysis (PCA). a) An initial NIR-II fluorescence image of a 4T1 tumor-bearing mouse before injection of 6PEG-Ag_2S QDs. b–g) NIR-II fluorescence images of the 4T1 tumor-bearing mouse at various time points after injection of 200 μL of 1.34 mg mL^{-1} 6PEG-Ag_2S QDs. h) A PCA overlaid image based on the continuous NIR-II fluorescence images. Lungs (blue); kidneys (red); tumor (green). Yellow arrows = 4T1 murine breast-cancer tumor. Note that in all images, the head of the mouse is at the top whereas the hind legs and tail are at the bottom. These results were reproduced with a total of three mice.

(Figure 2 d).[14] Besides the pulmonary and systemic circulations that could be clearly distinguished from the video-rate imaging, another interesting feature was the accumulation of NIR-II fluorescence signal in the tumor region, starting at approximately 15 s p.i. The NIR-II signal in the tumor region continued to increase from approximately 15 s p.i. to approximately 2 min p.i. (Figure 2 e–g). The vascular structure of the tumor also became distinguishable over time (compare Figure 2 f,g). Thus, video-rate NIR-II fluorescence imaging based on 6PEG-Ag_2S QDs afforded pinpointing of the location of the tumor within 2 min post injection.

To further distinguish the organs and the tumor based on dynamic contrast, principal component analysis (PCA)[6b,15] was applied to the first 100 frames (up to 11.9 s p.i.). The PCA overlaid image (Figure 2 h) after computation showed three distinct components (coded with orthogonal false-colors), corresponding to the lungs (blue), kidneys (red), and tumor (green). PCA grouped pixels into a component with similar time-dependent intensity-change profiles, and therefore was

able to discriminate various organs as QDs circulated through the organs. Owing to the dynamic contrast, PCA was more sensitive in locating the tumor within a shorter time post injection than the video-rate imaging (approximately 12 s p.i. for PCA versus approximately 2 min p.i. for real-space video imaging).

We monitored the NIR-II signal, which reflected the distribution of 6PEG-Ag_2S QDs inside the mouse, over a longer period of time up to 24 h post tail-vein injection (Figure 3 a–e, Figure S3,S4). Because of the enhanced permeability and retention (EPR) effect of the tumor vasculature,[12a] a steady increase of NIR-II fluorescence of 6PEG-Ag_2S QDs in the tumor region and a decrease of NIR-II fluorescence in other organs and skin was observed from 30 min p.i. to 24 h p.i., leading to an increased tumor-to-background ratio (TBR) over time (Figure 3). The TBR was well above the Rose criterion of 5 for 4–24 h p.i., indicating a positive imaging and detection of the tumor.[16] Visual inspection of the same mouse also showed high uptake of Ag_2S QDs in the tumor area that darkened from QD accumulation at 24 h p.i. (Figure 3 f).

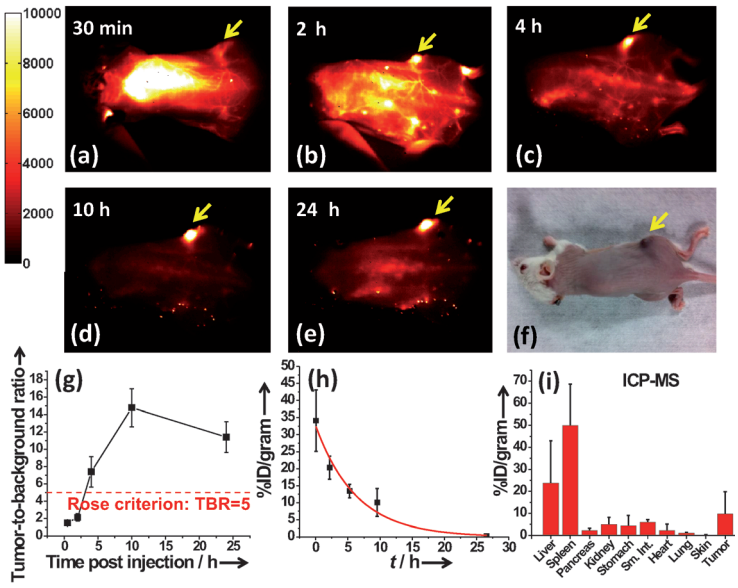

Figure 3. NIR-II fluorescence imaging of a xenograft 4T1 tumor with high uptake of 6PEG-Ag_2S QDs. (a–e) Time course of NIR-II fluorescence images of the same mouse injected with 6PEG-Ag_2S QDs in Figure 2. These results were reproduced with a total of three mice. f) A white-light optical image of the same mouse at 24 h p.i. The tumor mass was visibly darkened owing to high uptake of 6PEG-Ag_2S QDs. g) The tumor-to-background ratio (TBR) plotted as a function of time p.i. for NIR-II images, indicating a 100% certainty of the tumor being identified from the NIR-II image after 4 h p.i., according to the Rose criterion. h) A representative plot of the % ID/gram of the 6PEG-Ag_2S QDs in the blood versus time after tail-vein injection, as determined by the NIR-II fluorescence of the blood samples. A first-order exponential fits the data points with a half-life of circulation for the 6PEG-Ag_2S QDs of 4.37 ± 0.75 h. This half-life measurement was repeated with two other mice (3.98 ± 1.16 h and 3.51 ± 0.86 h, see Figure S5). i) Quantitative biodistribution of 6PEG-Ag_2S QDs in various organs and the tumor 72 h after injection based on ICP-MS.

To evaluate the effectiveness of the biocompatible surface coating of Ag_2S QDs, blood-circulation half-life of the 6PEG-Ag_2S QDs was determined to be 4.37 ± 0.75 h based on a fit to first-order exponential decay of the NIR-II fluorescence intensity of the blood samples (Figure 3 h), suggesting high biocompatibility and slow uptake by the reticuloendothelial system (RES) compared to the half-life of linear PEG-coated QDs ($t_{1/2} < 12$ min for CdSe/ZnS-PEG_{750} and $t_{1/2} \approx 2$ h for CdSe/ZnS-PEG_{5000}).[12c,17] To quantify the biodistribution of the 6PEG-Ag_2S QDs, mouse organs were collected 72 h after injection, when most of the injected QDs had stopped circulating in the blood. The QD biodistribution in the organs was found by two independent methods based on NIR-II fluorescence (Figure S6) and inductively coupled plasma-mass spectrometry (ICP-MS) (Figure 3 i). The 6PEG-Ag_2S QDs ended up primarily in the RES organs including the liver and spleen, while the tumor uptake of the 6PEG-Ag_2S QDs measured by the ICP-MS method was approximately 10% ID/gram, where % ID/gram indicates the probe concentration in terms of the percentage of the injected dose (ID) per gram of tissue. The non-targeted (passive) tumor uptake of approximately 10% ID/gram was one of the highest tumor uptake values reported to date for intravenously injected QDs. The highest reported % ID/gram tumor uptake of quantum dots, based on fluorescence intensity, was approximately 20% ID/gram at 4 h p.i. and dropped to 7% by 24 h p.i. for dendron-coated InP/ZnS core–shell QDs.[18] In contrast, the 6PEG-Ag_2S QDs maintain a 10% ID/gram tumor accumulation even at 72 h p.i., based on ICP-MS. The relatively long circulation time and high tumor uptake indicated that the 6PEG-Ag_2S QDs were well-coated with branched PEG functional groups, which limited the opsonization of proteins for rapid RES uptake.

As with any newly introduced in vivo nanomaterial, long term retention and toxicity are of concern. A separate in vivo toxicology study of 6PEG-Ag_2S QDs has shown minimal toxicity at a dose up to 1.68 nmol per mouse (that is, more than twofold higher than used in this work and still lower than the median toxic dose TD_{50}) over a period of two months as evidenced by blood biochemistry, hematological analysis, and histological examinations. Nevertheless, to gain a better understanding of the clearance pathway of this novel NIR-II fluorophore from the body, we studied the short-term retention and excretion after a single-dose injection of the 6PEG-Ag_2S QDs into tumor-free BALB/c mice ($n = 4$). Feces and urine were collected on a daily basis for quantitative measurement of Ag_2S QDs based on ICP-MS. Figure 4 a,b show the excretion of 6PEG-Ag_2S QDs mainly through the biliary pathway at a steady rate, which was expected because the hydrodynamic radius of the 6PEG-Ag_2S QDs was approximately 26.8 nm according to dynamic light scattering (DLS; Figure 4 d), far larger than the renal filtration cut-off size of 5 nm.[19] The biodistribution of the 6PEG-Ag_2S QDs was also examined at 24 h and 168 h (7 days) p.i. (Figure 4 c). By seven

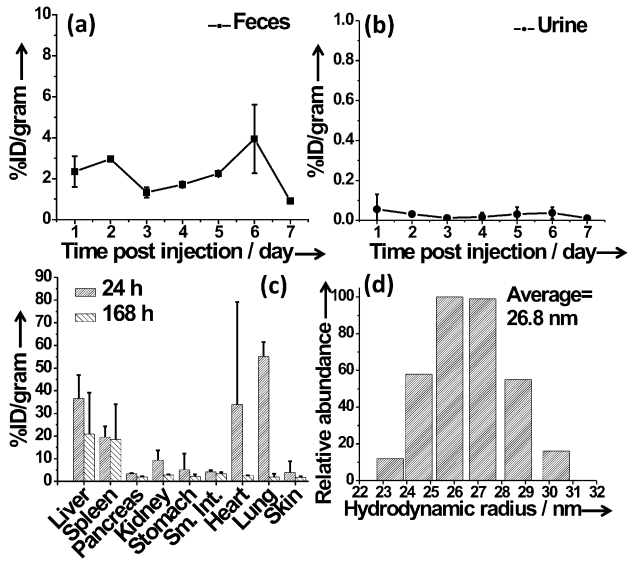

Figure 4. Short-term retention and excretion study of 6PEG-Ag_2S QDs measured by ICP-MS. a) The amount of 6PEG-Ag_2S QDs in feces collected from mice ($n=2$) housed in metabolic cages every 24 h for 7 days. b) The amount of 6PEG-Ag_2S QDs in urine collected in a similar manner from the mice. c) Biodistribution taken for two mice at 24 h p.i. and another two mice taken at 168 h p.i. d) Hydrodynamic-radius distribution of 6PEG-Ag_2S QDs based on DLS, indicating an average radius of 6PEG-Ag_2S QDs of 26.8 nm.

days p.i., the Ag_2S QDs were nearly cleared from all organs aside from the liver and the spleen.

In summary, we have developed biocompatible, heavy-metal free 6PEG-Ag_2S QDs as an imaging contrast agent that are brightly fluorescent in the NIR-II window. Imaging with these NIR-II QDs afforded deep inner organ registration, dynamic tumor contrast, and fast tumor detection. The in vivo pharmacokinetics of the QDs was studied, suggesting an unprecedented degree of accumulation of 6PEG-Ag_2S QDs in the tumor (>10% ID/gram) through the EPR effect. The short-term excretion profile of the 6PEG-Ag_2S QDs suggested biliary clearance as the main clearance pathway. Further studies of genotoxicity and reproductive toxicity will be used to evaluate the potential of this new type of NIR-II fluorophores for pre-clinical use.

Received: July 29, 2012
Published online: September 5, 2012

Keywords: fluorescence · in vivo imaging · quantum dots · second near-infrared window · tumor imaging

[1] A. Rosengren, L. Wilhelmsen, *Eur. J. Epidemiol.* **2004**, *19*, 533–540.
[2] S. Adams, R. P. Baum, T. Stuckensen, K. Bitter, G. Hor, *Eur. J. Nucl. Med.* **1998**, *25*, 1255–1260.
[3] L. V. Wang, H.-I. Wu, *Biomedical optics: principles and imaging*, Wiley, Hoboken, **2007**.
[4] G. M. van Dam, G. Themelis, L. M. A. Crane, N. J. Harlaar, R. G. Pleijhuis, W. Kelder, A. Sarantopoulos, J. S. de Jong, H. J. G. Arts, A. G. J. van der Zee, J. Bart, P. S. Low, V. Ntziachristos, *Nat. Med.* **2011**, *17*, 1315–1319.
[5] a) K. Welsher, Z. Liu, D. Daranciang, H. Dai, *Nano Lett.* **2008**, *8*, 586–590; b) G. S. Hong, S. M. Tabakman, K. Welsher, Z. Chen, J. T. Robinson, H. L. Wang, B. Zhang, H. J. Dai, *Angew. Chem.* **2011**, *123*, 4740–4744; *Angew. Chem. Int. Ed.* **2011**, *50*, 4644–4648; c) G. S. Hong, J. Z. Wu, J. T. Robinson, H. L. Wang, B. Zhang, H. J. Dai, *Nat. Commun.* **2012**, *3*, 700.
[6] a) K. Welsher, Z. Liu, S. P. Sherlock, J. T. Robinson, Z. Chen, D. Daranciang, H. J. Dai, *Nat. Nanotechnol.* **2009**, *4*, 773–780; b) K. Welsher, S. P. Sherlock, H. J. Dai, *Proc. Natl. Acad. Sci. USA* **2011**, *108*, 8943–8948; c) Z. Liu, S. Tabakman, K. Welsher, H. J. Dai, *Nano Res.* **2009**, *2*, 85–120; d) J. T. Robinson, K. Welsher, S. M. Tabakman, S. P. Sherlock, H. L. Wang, R. Luong, H. J. Dai, *Nano Res.* **2010**, *3*, 779–793; e) J. T. Robinson, G. S. Hong, Y. Y. Liang, B. Zhang, O. K. Yaghi, H. J. Dai, *J. Am. Chem. Soc.* **2012**, *134*, 10664–10669.
[7] a) A. M. Smith, M. C. Mancini, S. M. Nie, *Nat. Nanotechnol.* **2009**, *4*, 710–711; b) Y. T. Lim, S. Kim, A. Nakayama, N. E. Stott, M. G. Bawendi, J. V. Frangioni, *Mol. Imaging* **2003**, *2*, 50–64; c) J. V. Frangioni, *Curr. Opin. Chem. Biol.* **2003**, *7*, 626–634; d) A. N. Bashkatov, E. A. Genina, V. I. Kochubey, V. V. Tuchin, *J. Phys. D* **2005**, *38*, 2543–2555.
[8] M. J. O'Connell, S. M. Bachilo, C. B. Huffman, V. C. Moore, M. S. Strano, E. H. Haroz, K. L. Rialon, P. J. Boul, W. H. Noon, C. Kittrell, J. P. Ma, R. H. Hauge, R. B. Weisman, R. E. Smalley, *Science* **2002**, *297*, 593–596.
[9] a) Y. P. Du, B. Xu, T. Fu, M. Cai, F. Li, Y. Zhang, Q. B. Wang, *J. Am. Chem. Soc.* **2010**, *132*, 1470–1471; b) S. Shen, Y. Zhang, L. Peng, B. Xu, Y. Du, Q. B. Wang, *Angew. Chem.* **2011**, *123*, 7253–7256; *Angew. Chem. Int. Ed.* **2011**, *50*, 7115-7118; c) L. Bakueva, I. Gorelikov, S. Musikhin, X. S. Zhao, E. H. Sargent, E. Kumacheva, *Adv. Mater.* **2004**, *16*, 926–929.
[10] a) R. Pizzoferrato, M. Casalboni, F. De Matteis, P. Prosposito, *J. Lumin.* **2000**, *87–89*, 748–750; b) O. E. Semonin, J. C. Johnson, J. M. Luther, A. G. Midgett, A. J. Nozik, M. C. Beard, *J. Phys. Chem. Lett.* **2010**, *1*, 2445–2450.
[11] Y. Zhang, G. S. Hong, Y. J. Zhang, G. C. Chen, F. Li, H. J. Dai, Q. B. Wang, *ACS Nano* **2012**, *6*, 3695–3702.
[12] a) X. H. Gao, Y. Y. Cui, R. M. Levenson, L. W. K. Chung, S. M. Nie, *Nat. Biotechnol.* **2004**, *22*, 969–976; b) D. R. Larson, W. R. Zipfel, R. M. Williams, S. W. Clark, M. P. Bruchez, F. W. Wise, W. W. Webb, *Science* **2003**, *300*, 1434–1436; c) B. Ballou, B. C. Lagerholm, L. A. Ernst, M. P. Bruchez, A. S. Waggoner, *Bioconjugate Chem.* **2004**, *15*, 79–86.
[13] R. Matthes, et al. *Health Phys.* **2000**, *79*, 431–440.
[14] By the staff of the Jackson Laboratory: B. H. M. Roscoe, B. Jackson, *Biology of the laboratory mouse* (Eds.: E. L. Green, D. L. Coleman, E. U. Fahay), 2nd ed., McGraw-Hill, New York, **1966**.
[15] E. M. C. Hillman, A. Moore, *Nat. Photonics* **2007**, *1*, 526–530.
[16] J. T. Bushberg, *The essential physics of medical imaging*, Lippincott Williams & Wilkins, **2002**.
[17] W. T. Al-Jamal, K. T. Al-Jamal, A. Cakebread, J. M. Halket, K. Kostarelos, *Bioconjugate Chem.* **2009**, *20*, 1696–1702
[18] J. H. Gao, K. Chen, R. Luong, D. M. Bouley, H. Mao, T. C. Qiao, S. S. Gambhir, Z. Cheng, *Nano Lett.* **2012**, *12*, 281–286.
[19] L. F. Qi, X. H. Gao, *Expert Opin. Drug Delivery* **2008**, *5*, 263–267.

